Runge-Kutta Approximation of a Non-Linear Wing Flutter System

Golemis, Shaun [*] , Kemp, John [†] , Ochs, Ben [‡] , Peters, Karsten [§] , and Veranga, Joshua [¶]
University of Illinois at Urbana-Champaign, Champaign, IL 61801, USA

This report presents the design and implementation of the Runge-Kutta (RK4) numerical method in order to approximate the non-linear wing flutter of an aircraft. The approximation aims to estimate the amount of time until the aircraft reaches a divergence from a set of initial conditions corresponding to specific perturbations. RK4 was chosen due to its ability to solve ordinary differential equations with very high accuracy while having relatively low computational cost. To estimate the equilibrium time, we linearized the structural and aerodynamic models of flutter where lift and the moment are modeled using thin airfoil theory. After running calculations, we found that the speed of divergence is 50 $\mathrm{m\,s^{-1}}$**.**

I. Nomenclature

m	=	mass per unit span, $\frac{\mathrm{kg}}{\mathrm{m}}$
I_α	=	pitch moment of inertia per unit span, $\frac{\mathrm{kg\cdot m^2}}{\mathrm{m}}$
k_h	=	plunge (heave) stiffness per unit span, $\frac{\mathrm{N}}{\mathrm{m^2}}$
k_θ	=	pitch stiffness per unit span, $\frac{\mathrm{N\cdot m}}{\mathrm{rad\cdot m}}$
S_α	=	aerodynamic coupling coefficient, kg
$h(t)$, $\dot{h}(t)$, $\ddot{h}(t)$	=	plunge displacement, velocity, and acceleration, m, $\frac{\mathrm{m}}{\mathrm{s}}$, $\frac{\mathrm{m}}{\mathrm{s^2}}$
$\theta(t)$, $\dot{\theta}(t)$, $\ddot{\theta}(t)$	=	pitch angle, rate, and angular acceleration, rad, $\frac{\mathrm{rad}}{\mathrm{s}}$, $\frac{\mathrm{rad}}{\mathrm{s^2}}$
$L(t)$	=	aerodynamic lift force per unit span, $\frac{\mathrm{N}}{\mathrm{m}}$
$M(t)$	=	aerodynamic moment per unit span, $\frac{\mathrm{N\cdot m}}{\mathrm{m}}$
U	=	freestream velocity, $\frac{\mathrm{m}}{\mathrm{s}}$
ρ	=	air density, $\frac{\mathrm{kg}}{\mathrm{m^3}}$
b	=	semi-chord length of the airfoil, m
C_{L_α}	=	lift curve slope, dimensionless
C_{M_α}	=	moment curve slope, dimensionless
$y(t)$	=	state vector $[h, \dot{h}, \theta, \dot{\theta}]^\mathsf{T}$
$f(t, y)$	=	right-hand side vector field for the ODE system
k_1, k_2, k_3, k_4	=	intermediate slopes in Runge-Kutta method
atol, rtol	=	absolute and relative tolerance

II. Introduction

Flutter is a complex aeroelastic phenomenon that occurs when the interaction between aerodynamic forces and structural dynamics leads to self-excited oscillations. This instability can result in catastrophic failure if not carefully predicted and mitigated, particularly in lightweight, flexible structures such as unmanned aerial vehicle (UAV) wings, high-aspect-ratio wings, and control surfaces. Understanding the onset and behavior of flutter is essential in the design and safety analysis of these structures.

In this study, we examine the non-linear dynamics of wing flutter using the pitch–plunge model, a simplified representation that captures the coupled interaction between a wing's vertical displacement (plunge) and angular motion

[*]BS Student, Aerospace Engineering, Grainger College of Engineering, 104 S Wright St, Urbana, Illinois 61820, golemis2@illinois.edu
[†]BS Student, Aerospace Engineering, Grainger College of Engineering, 104 S Wright St, Urbana, Illinois 61820, jwkemp2@illinois.edu
[‡]BS Student, Aerospace Engineering, Grainger College of Engineering, 104 S Wright St, Urbana, Illinois 61820, bochs2@illinois.edu
[§]BS Student, Aerospace Engineering, Grainger College of Engineering, 104 S Wright St, Urbana, Illinois 61820, kjp@illinois.edu
[¶]BS Student, Aerospace Engineering, Grainger College of Engineering, 104 S Wright St, Urbana, Illinois 61820, veranga2@illinois.edu

(pitch). This system of second-order differential equations exhibits inherent non-linearities, which prevent closed-form solutions, necessitating the use of numerical methods for accurate analysis.

To approximate the solution to this nonlinear system, we apply the fourth-order Runge-Kutta (RK4) method, a widely recognized and efficient numerical integration technique. RK4 offers high accuracy while maintaining computational feasibility, making it an ideal method for solving the coupled differential equations governing flutter dynamics. By employing RK4, we can simulate the system's time evolution and explore the effects of key parameters, such as the freestream velocity, structural stiffness, and moment of inertia, on system stability. The primary objective of this study is to determine at what velocity flutter begins for a given set of wing parameters and how the wing behaves.

The results of this study provide a comprehensive understanding of the non-linear dynamics of wing flutter and contribute to the development of better predictive models and control strategies for aeroelastic systems in aerospace engineering.

III. Methodology

A. Governing Equations

We consider the unsteady dynamics of a two-degree-of-freedom (2-DOF) aeroelastic system consisting of a lifting surface capable of plunging and pitching. The linearized structural and aerodynamic model captures the essential physics of flutter and is given by the coupled second-order system:

$$\begin{aligned} m\ddot{h}(t) + k_h h(t) &= L(t) - S_\alpha \dot{\theta}(t), \\ I_\alpha \ddot{\theta}(t) + k_\theta \theta(t) &= M(t) - S_\alpha \ddot{h}(t), \end{aligned} \tag{1}$$

where $h(t)$ is the plunge displacement, $\theta(t)$ is the pitch angle, m and I_α are the mass and pitch moment of inertia, and k_h, $k_t h$, S_α are the stiffness and aerodynamic coupling coefficients. Additionally, the aerodynamic lift $L(t)$ and the moment $M(t)$ are modeled using quasi-steady thin airfoil theory, expressed as:

$$\begin{aligned} L(t) &= \rho U^2 b C_{L_\alpha} \left(\theta(t) + \frac{\dot{h}(t)}{U} \right), \\ M(t) &= \rho U^2 b^2 C_{M_\alpha} \left(\theta(t) + \frac{\dot{h}(t)}{U} \right), \end{aligned} \tag{2}$$

with U the freestream velocity, ρ the fluid density, and b the semi-chord. The system is then reformulated into a first-order ODE system by defining the state

$$y(t) = \begin{bmatrix} h(t) \\ \dot{h}(t) \\ \theta(t) \\ \dot{\theta}(t) \end{bmatrix} \in \mathbb{R}^4 \tag{3}$$

where the right-hand side function $f(t, y$ is then constructed using the above dynamics to yield

$$\dot{y}(t) = f(t, y(t); \text{params}), \tag{4}$$

which forms the basis for the time-domain numerical integration.

B. Time Integration Method

To solve the system, we employ both the classical fourth-order Runge-Kutta (RK4)[1] method and an adaptive Runge-Kutta-Fehlberg 4(5) (RK45)[2] method based on the Dormand-Prince tableau[3]. The RK4 method advances the

solution over a time step of h via:

$$\begin{aligned} k_1 &= f(t, y), \\ k_2 &= f\left(t = \frac{h}{2}, y + \frac{h}{2}k1\right), \\ k_3 &= f\left(t + \frac{h}{2}, y + \frac{h}{2}k_2\right), \\ k_4 &= f(t + h, y + hk_3), \\ y(t + h) &= y(t) + \frac{h}{6}(k_1 + 2k_2 + 2k_3 + k_4) \end{aligned} \tag{5}$$

thus conveying the method having a local truncation error $O\left(h^5\right)$ and a global error $O\left(h^4\right)$. Therefore, for improved robustness and step size control, RK45 is implemented using the Dormand–Prince coefficients. The method computes both 4th- and 5th-order estimates $y^{(4)}$, $y^{(5)}$, and utilizes the RMS scaled error estimate:

$$\varepsilon = \sqrt{\frac{1}{n}\sum_{i=1}^{n}\left(\frac{y_i^{(5)} - y_i^{(4)}}{\text{atol} + \text{rtol} \cdot \max\left(|y_i|, \left|y_i^{(5)}\right|\right)}\right)} \tag{6}$$

to adapt to the step size via:

$$h_{new} = h \cdot \min\left(\max\left(0.2, 0.9 \cdot \varepsilon^{-0.2}\right), 5.0\right) \tag{7}$$

IV. Convergence and Verification

To verify the correct implementation of our numerical methods, we conducted a convergence study using the fixed-step RK4 solver. Although the primary simulations use the adaptive RK45 method, RK4 offers a straightforward framework to test for the expected error scaling without the complexity of adaptive step sizes.

We integrate the system over a short time interval $[0, 2]$ seconds using a sequence of decreasing step sizes $h = \{0.2, 0.1, 0.05, 0.025, 0.0125\}$. For each step size, we compute the solution $y_h(t_f)$ at the final time $t_f = 2$ and compare it to a reference solution $y_{\text{ref}}(t_f)$ obtained using a very small step size ($h = 10^{-4}$). The relative error is computed as:

$$\text{Error}(h) = \frac{\left\|y_h(t_f) - y_{\text{ref}}(t_f)\right\|_2}{\left\|y_{\text{ref}}(t_f)\right\|_2} \tag{8}$$

Figure 1 shows a log-log plot of the error as a function of step size. The slope of the error curve is approximately 4, which confirms the expected fourth-order convergence rate of the RK4 method. This agreement with theoretical scaling validates the correctness of the solver implementation.

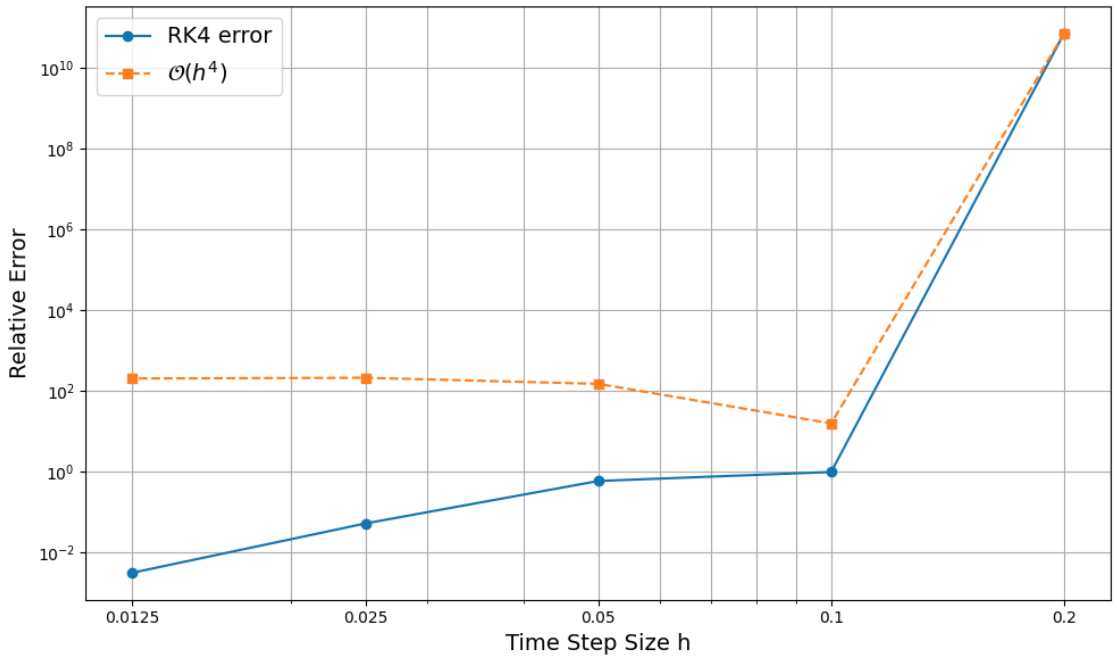

Fig. 1 Convergence of RK4 solver: error vs. time step size h on a log-log scale.

Furthermore, during flutter simulations, the RK45 method was observed to adaptively refine the time step as the instability developed, maintaining bounded error throughout. This provides qualitative validation of the error control mechanism in the Dormand–Prince scheme.

V. Results and Discussion

Table 1 Baseline wing parameters used in flutter simulations.

Parameter	Description	Value
ρ	Air density	$1.225\ \text{kg/m}^3$
b	Semi-chord length	0.5 m
m	Mass per unit span	100.0 kg/m
I_α	Pitch moment of inertia per unit span	$20.0\ \text{kg} \cdot \text{m}^2/\text{m}$
S_α	Aerodynamic coupling coefficient	0.0
k_h	Plunge stiffness per unit span	$5.0 \times 10^4\ \text{N/m}$
k_θ	Pitch stiffness per unit span	$2000.0\ \text{N} \cdot \text{m/rad}$
C_{L_α}	Lift curve slope	2π
C_{M_α}	Moment curve slope	-0.2π

The wing parameters listed in Table 1 define the structural and aerodynamic properties used in the simulations. The air density $\rho = 1.225\ \text{kg/m}^3$ corresponds to standard sea-level atmospheric conditions. The semi-chord length $b = 0.5$ m is appropriate for a medium-sized flexible wing and plays a role in determining the aerodynamic moment arm. The structural mass per unit span $m = 100\ \text{kg/m}$ and moment of inertia $I_\alpha = 20.0\ \text{kg} \cdot \text{m}^2/\text{m}$ were chosen to ensure a reasonably stiff and heavy system, allowing us to observe flutter onset within a manageable velocity range. The plunge stiffness $k_h = 5.0 \times 10^4\ \text{N/m}$ and pitch stiffness $k_\theta = 2000\ \text{N} \cdot \text{m/rad}$ reflect realistic values for aircraft wing sections with moderate structural rigidity. The aerodynamic coupling coefficient S_α is set to zero to isolate the effects of

structural and aerodynamic stiffness without additional coupling between translational and rotational accelerations. Aerodynamic force generation is modeled using thin airfoil theory. The lift curve slope $C_{L_\alpha} = 2\pi$ is the classical result for a symmetric thin airfoil at low angles of attack. The moment curve slope $C_{M_\alpha} = -0.2\pi$ reflects a modest nose-down pitching moment with increasing angle of attack, typical for symmetric airfoils with a quarter-chord moment reference. These parameters collectively define a physically representative aeroelastic system that balances simplicity with realism, enabling both qualitative and quantitative exploration of flutter dynamics.

With confidence in our numerical solvers, we proceeded to explore the flutter behavior under varying freestream velocities. The simulations revealed that for velocities below approximately 50 $\mathrm{m\,s^{-1}}$, the system exhibited stable oscillations that gradually decayed over time, see figure 2. At these lower velocities, both the plunge and pitch displacements remained bounded, and the dynamics were characterized by damping behavior.

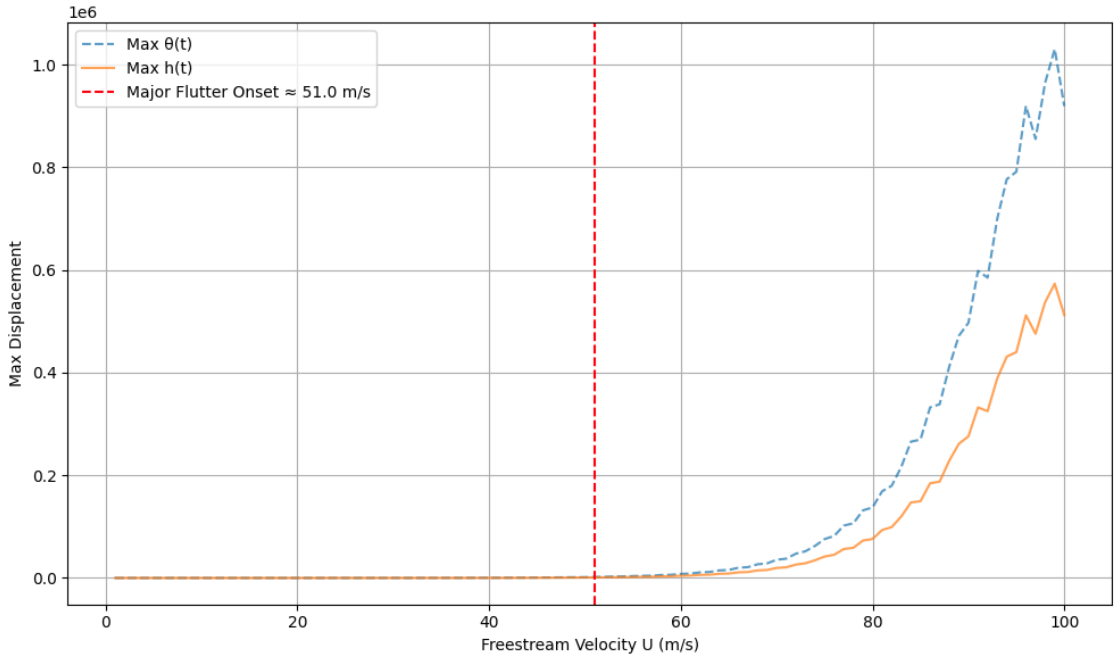

Fig. 2 Plot of the wing pitch and plunge as wing velocity increases with instability occurring at 50 $\mathrm{m\,s^{-1}}$.

In contrast, when the freestream velocity was increased beyond 50 $\mathrm{m\,s^{-1}}$, the system became unstable, displaying growing oscillations and eventual divergence. At 60 $\mathrm{m\,s^{-1}}$ see figure 3, for example, the pitch angle exceeded 0.1 radians within two seconds, with the plunge motion similarly diverging. This indicates that the critical flutter velocity lies between 50 $\mathrm{m\,s^{-1}}$ and 60 $\mathrm{m\,s^{-1}}$ for the chosen baseline parameters. This behavior is consistent with theoretical expectations for aeroelastic systems, where increased aerodynamic loading at higher velocities can overpower structural damping and stiffness, leading to self-excited oscillations.

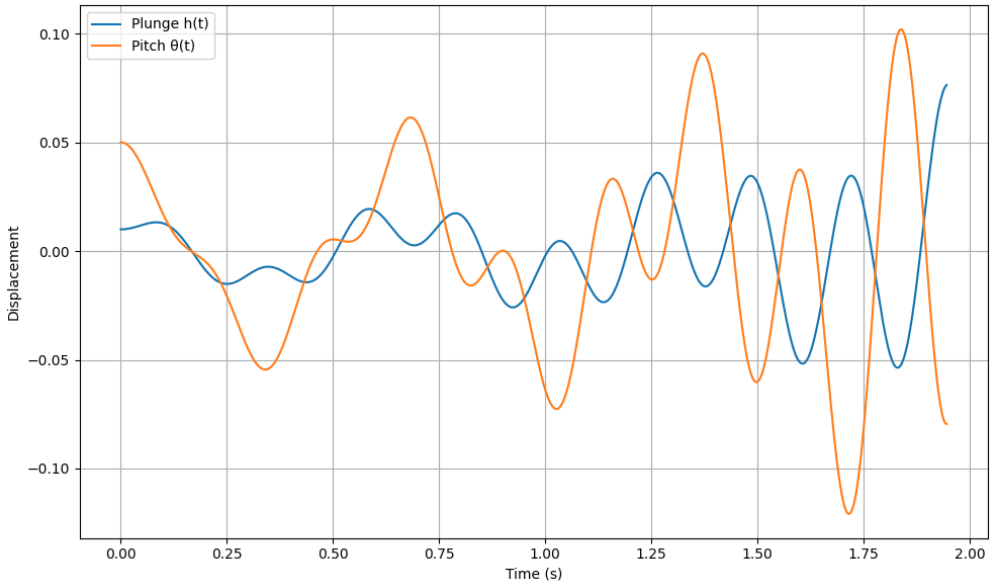

Fig. 3 Wing flutter over 2 seconds at 60 $\mathrm{m\,s^{-1}}$.

Figure 4 provides a visual depiction* of the wing's dynamic state at a freestream velocity of 60 $\mathrm{m\,s^{-1}}$, where the flutter instability is fully developed. In this figure, the wing is represented as a line evolving over time, where both the vertical position and the angle of the line correspond to the plunge displacement $h(t)$ and pitch angle $\theta(t)$, respectively. As time progresses, the increasing vertical motion of the line reflects growing plunge amplitude, while the rotation of the line about its center illustrates the pitch motion. The amplitude of both motions increases rapidly and nonlinearly, indicating that the wing is undergoing large, self-excited oscillations characteristic of post-flutter behavior. Initially small disturbances amplify exponentially, and by the final frames, the wing shows extreme deflection and rotation—hallmarks of a divergent response. This visualization clearly conveys the physical manifestation of flutter: the coupled interaction between vertical translation and angular rotation that can lead to structural instability. The figure underscores the importance of predicting flutter onset and highlights how even simple visualizations can offer powerful insight into complex aeroelastic phenomena.

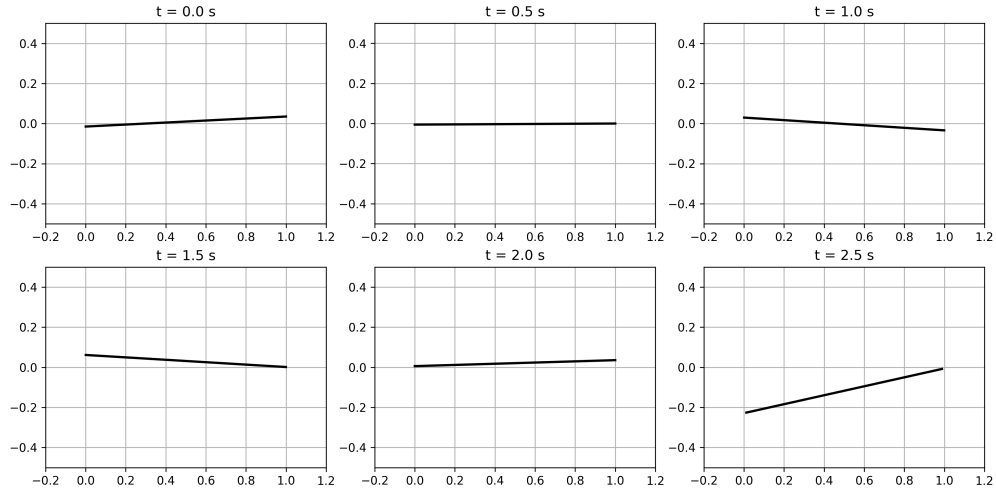

Fig. 4 Visual frames of wing flutter at different time steps.

*Full animation can be found in Git repository — see **Appendix.A**

VI. Conclusion

In this study, we utilized the Runge-Kutta method, specifically RK4, to model and analyze the non-linear dynamics of wing flutter in an aeroelastic system. By examining the effects of various parameters, including freestream velocity and structural stiffness, we determined that the critical flutter velocity for the selected wing configuration was approximately 50 $\mathrm{m\,s^{-1}}$. Below this velocity, the wing displayed stable oscillations with decaying amplitudes, while above this threshold, the system became unstable, leading to rapidly growing oscillations and divergence. This behavior aligns with theoretical expectations, where increased aerodynamic loading at higher speeds induces self-excited oscillations that can compromise the structural integrity of the wing. The use of adaptive step-size methods, such as RK45, allowed for efficient and accurate time-domain simulations, providing valuable insights into the onset of flutter and the potential for further aeroelastic optimization in aircraft design. The findings underscore the importance of accurately predicting flutter behavior for safe and reliable aircraft operation.

Appendix

A. Git Repository

The respective Git repository where you can find the project code workflow published unequivocally for modularity and reproducibility.

B. Roles

1. Golemis, Shaun

19% contribution (1 & 4)

Did initial code generation with ChatGPT and helped modify. Wrote the results and discussion and conclusion with Ben, Karsten, and ChatGPT.

2. Kemp, John

19% contribution (1 & 2)

Wrote the nomenclature, introduction, and appendix sections with assistance from ChatGPT. Helped to format the sections of the paper in AIAA format.

3. Ochs, Ben

19% contribution (1 & 4)

Helped generate and modify the initial code generated to fit the problem better. Wrote the results and discussion and conclusion with Shaun, Karsten, and ChatGPT.

4. Peters, Karsten

19% contribution (1 & 3 & 4)

Wrote abstract and helped write results and conclusion with Ben and Shaun. Also helped modify code using ChatGPT.

5. Veranga, Joshua

24% contribution (2 & 3)

Wrote the methodology and convergence sections based on the workflow of the generated code. Helped to modify the code and ultimately finalized it to be published in the Git repository.

Acknowledgments

Special thanks are due to Dr. Goza, the TA/CA staff, and ChatGPT for their invaluable guidance and expertise throughout the project. ChatGPT took the prompts we generated and created the initial code base all of our work is based on and it was consulted during the writing of this report. We also wish to acknowledge the support of the Department of Aerospace Engineering for providing the resources necessary for this research.

References

[1] Butcher, J. C., *Numerical Methods for Ordinary Differential Equations*, 3rd ed., John Wiley & Sons, 2016.

[2] Dormand, J. R., and Prince, P. J., "A family of embedded Runge-Kutta formulae," *Journal of Computational and Applied Mathematics*, Vol. 6, No. 1, 1980, pp. 19–26.

[3] Hairer, E., N$\omega rsett, S. P., and Wanner, G.$, *Solving Ordinary Differential Equations I: Nonstiff Problems*, $Vol.$ 8, $Springer$, 1993.